

## Full Length Article

# Photocatalytic glucose electrooxidation of titanium dioxide doped CdTe enhanced for a photocatalytic fuel cell

Aykut Caglar<sup>a</sup>, Nahit Aktas<sup>a,b,\*</sup>, Hilal Kivrak<sup>b,c,d,\*</sup>

<sup>a</sup> Van Yuzuncu Yil University, Faculty of Engineering, Department of Chemical Engineering, Van, Turkey

<sup>b</sup> KyrgyzTurk Manas University, Faculty of Engineering, Department of Chemical Engineering, Bishkek, Kyrgyzstan

<sup>c</sup> Eskisehir Osmangazi University, Faculty of Engineering and Architectural Sciences, Department of Chemical Engineering, Eskisehir, Turkey

<sup>d</sup> Translational Medicine Research and Clinical Center, Eskisehir Osmangazi University, Eskisehir, Turkey



## ARTICLE INFO

## Keywords:

Cadmium  
Tellurium  
Titanium dioxide  
Photocatalysts  
Photocatalytic fuel cell

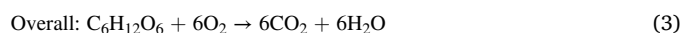
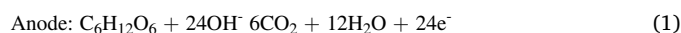
## ABSTRACT

The 0.1 % CdTe/TiO<sub>2</sub> photocatalysts with different atomic molar ratios (90–10, 70–30, 50–50, and 30–70) were synthesized by the wetness impregnation method and characterized by the XRD, SEM-EDX and mapping, N<sub>2</sub> adsorption–desorption, ICP-MS, TEM-EDS and STEM mapping, UV–VIS spectroscopy, fluorescence spectroscopy, XPS, TPR, TPO, and TPD analyses. The photocatalytic activities were examined to investigate by CV, CA, and EIS electrochemical analyses for photocatalytic fuel cells (PFCs) in glucose solution in the dark and under UV illumination. The characterization analyses revealed that anatase TiO<sub>2</sub> was formed for the catalyst and changed its electronic structure and surface properties when doped with metal. The photocatalytic glucose electrooxidation results indicated that the 0.1 % CdTe(50–50)/TiO<sub>2</sub> catalyst exhibited much higher photocatalytic activity, stability, and resistance than other catalysts both in the dark (6.22 mA cm<sup>-2</sup>) and under UV illumination (16.88 mA cm<sup>-2</sup>). The study offered a promising new type of photocatalysts for PFC applications.

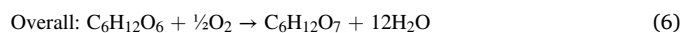
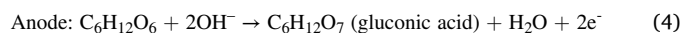
## 1. Introduction

The demand for energy in the world is met by non-renewable fossil fuel (oil, coal, and natural gas, etc.) resources [1]. The researchers have turned to alternative energy sources due to the limited use of fossil energy sources and the formation of harmful gases such as carbon dioxide, sulfur oxide, and nitric oxide to the environment as a result of use of these energy sources. Therefore, fuel cells as clean energy sources have attracted the attention of the scientific world to meet the world's energy demand as one of the most important energy sources of the future. Fuel cells hold promise as a sustainable and efficient energy source for a clean future that converts chemical energy directly into electrical energy [2,3]. Photocatalytic fuel cells (PFCs) that semiconductor photoanode, cathode, and electrolyte-containing such as methanol [4], ethanol [5], glucose (C<sub>6</sub>H<sub>12</sub>O<sub>6</sub>) [6] are promising devices that can handle with the energy crisis and environmental pollution utilizing sunlight as energy input. Glucose is a high energy density (4.43 kWh/kg), non-toxic, flammable, and non-volatile, potential hydrogen carrier and is the most abundant simple sugar in nature [7]. A glucose molecule can produce 24 electrons and yield -2870 kJ/mol of energy via the

complete oxidation to CO<sub>2</sub> through the following chemical equations:



However, glucose is a very stable molecule, it is difficult to break down and oxidize, so more research is needed. It is worth noting that it consists mostly of gluconic acid and a two-electron generating system, as demonstrated in the following chemical reaction in all studies to date [8]:



In the catalytic oxidation of glucose, which is utilized as a renewable energy source to meet the energy demand, materials such as metal, metal oxide nanoparticles, enzymes, semiconductors have been widely

\* Corresponding authors at: Eskisehir Osmangazi University, Faculty of Engineering and Architectural Sciences, Department of Chemical Engineering, Eskisehir, Turkey.

E-mail addresses: [nahit.aktas@manas.edu.kg](mailto:nahit.aktas@manas.edu.kg), [naktas@yyu.edu.tr](mailto:naktas@yyu.edu.tr) (N. Aktas), [hilaldemir.kivrak@ogu.edu.tr](mailto:hilaldemir.kivrak@ogu.edu.tr) (H. Kivrak).

<https://doi.org/10.1016/j.fuel.2022.125653>

Received 17 December 2021; Received in revised form 28 July 2022; Accepted 13 August 2022

Available online 19 August 2022

0016-2361/© 2022 Elsevier Ltd. All rights reserved.

**Table 1**  
The comparison related to literature for glucose electrooxidation.

Anode Catalysts	Preparation Method	Current Density (mA cm <sup>-2</sup> )	Reference
CNT/nano-TiO <sub>2</sub> /Pt complex electrode	–	13.00	[25]
NiO-TiO <sub>2</sub> -ZrO <sub>2</sub> /SO <sub>4</sub> <sup>2-</sup>	Facile method	5.19	[26]
Cu/Cu <sub>2</sub> O/TNT	Electroplating method	6.40	[27]
Ni(OH) <sub>2</sub> -24.2 %/TNT	Hydrothermal method	23.43	[28]
Few layer graphene/ITO	Chemical vapor deposition method	6.58	[29]
N-doped few layer graphene/ITO	Chemical vapor deposition method	9.12	[30]
Pt-graphene/ITO	Chemical vapor deposition method	9.21	[31]
C doped-TNT (UV illumination)	Anodization method	9.10	[32]
0.1 % Cd/TiO <sub>2</sub> (UV illumination)	Wetness impregnation method	6.00	[33]

examined as catalysts [9]. Photocatalysis changes the rate of a chemical reaction when a semiconductor material is exposed to light. Semiconductor materials are photocatalysts that absorb light and act as catalysts for chemical reactions [10,11]. The materials such as titanium dioxide (TiO<sub>2</sub>), zinc oxide (ZnO), tin dioxide (SnO<sub>2</sub>) as semiconductor materials are used as photocatalysts in the literature [12–17]. TiO<sub>2</sub> (3.2 eV wide bandgap [18]), which was first discovered by Fujishima and Honda in 1972 with its water separation feature, was used as a photoanode [19].

TiO<sub>2</sub> has the disadvantage that it adsorbs less than 5 % of the solar source of UV light and causes rapid recombination of photogenerated electron-hole pairs, leading to low quantum yield and activity for PFCs. Researchers have been studied TiO<sub>2</sub>-based metals [20], metal sulfides [21], metal oxides [22], carbon-based materials [23] to improve their photocatalytic activities for PFCs. Hu et al [24] reported that they investigated the effects of photocatalytic degradation mechanisms of different organic classes and comprehensive characterization of photoelectrochemical properties by optimization of TiO<sub>2</sub>, WO<sub>3</sub>, and Nb<sub>2</sub>O<sub>5</sub> photoanodes with statistical 2 k factorial design for PFCs. They emphasized that the TiO<sub>2</sub>-based PFC gives the highest photocurrent density as a result of its high intrinsic quantum efficiency compared to the others. Table 1 summarizes current densities values of the different materials compiled from the literature for glucose electrooxidation. It can be shown in Table 1 that apart from a few studies as PFCs, there are only studies on glucose fuel cells in the literature.

The catalytic performance of catalysts in literature has been examined in many fields such as water splitting [34], fuel cells [35], hydrogen

storage [36], supercapacitors [37], solar energy [38], lithium-ion batteries [39]. Photocatalytic performances of semiconductor materials such as TiO<sub>2</sub> with different metals have been investigated in many areas such as decomposition, hydrogen production, CO<sub>2</sub> reduction [40,41]. However, photocatalytic electrooxidation studies of photoanode catalysts for fuel cells are not available in the literature except for a few studies. Herein, TiO<sub>2</sub> supported CdTe photocatalysts were synthesized at different atomic molar ratios (90:10, 70:30, 50:50, 30:70) by using the impregnation method. The reduction process was realized in a furnace under argon gas at 400 °C. The XRD, SEM-EDX and mapping, TEM, XPS, UV-vis spectroscopy, fluorescence spectroscopy, TPR, TPO, and TPD analyses were used to examine the structure of catalysts. The CV, CA, and EIS analyses were realized to investigate the catalytic activity of photocatalytic glucose electrooxidation at dark and under UV illumination.

## 2. Experimental

### 2.1. Synthesis of CdTe/TiO<sub>2</sub> catalysts

All chemicals were bought from Sigma-Aldrich. CdTe/TiO<sub>2</sub> catalysts were synthesized in different ratios by using the wetness impregnation method. The wet impregnation method is a widely used catalyst synthesis method in which the metal precursor is dissolved in a solvent and mixed with the support material. It is a method for doping metals to the support material like the studies in the literature [42,43]. The Cd loading was adjusted to 0.1 % by the weight. Firstly, the appropriate amounts of Cd precursor (CdCl<sub>2</sub>·H<sub>2</sub>O, 99.995 %) and Te precursor (Na<sub>2</sub>O<sub>3</sub>Te, 99 %) were distributed under sonication with DI water in a beaker for 0.1 % CdTe/TiO<sub>2</sub> catalysts. After the metal precursors were homogeneously dispersed in DI water, TiO<sub>2</sub> (TiO<sub>2</sub>, 99 %) was added and mixed for 30–60 min with the help of a glass rod. It was then left to dry at 85 °C for overnight. Finally, the reduction process of the obtained catalysts was kept under argon gas for 2 h up to 400 °C at a heating rate of 10 °C/min in a furnace. Cooling was carried out with the help of a fan. 0.1 % CdTe/TiO<sub>2</sub> catalysts were synthesized under the same synthesis conditions with (90–10), (70–30), (50–50), and (30–70) metal ratios.

### 2.2. Characterization of CdTe/TiO<sub>2</sub> catalysts

The X-ray Diffraction (XRD) patterns were performed to examine crystal structures with an Empyrean (PANalytical) diffractometer using Cu-Kα (λ = 1.5406 Å) radiation source. The surface morphologies of catalysts were characterized utilizing SEM-EDX and mapping (ZEISS Sigma 300) analysis. N<sub>2</sub> adsorption-desorption analyses were realized on a Micromeritics Tristar II 3020 equipped with a surface area and porosity measurement analyzer. The atomic ratios of the catalysts were defined with ICP-MS by using Agilent 7800 device. TEM analysis was obtained using the Hitachi HighTech HT7700 device at 120 kV accelerating voltage and a maximum resolution of 0.204 nm. UV-VIS spectra were recorded utilizing the Shimadzu UV-3600 Plus device. The fluorescence spectrum of catalysts was measured by a Perkin Elmer FL6500 fluorescence spectrophotometer. The elemental composition and oxidation state of the 0.1 % CdTe(50–50)/TiO<sub>2</sub> catalyst were examined using XPS analysis (Specs-Flex) with a CCD detector (Kα (Al): 1486.7 eV). Micromeritics Chemisorb 2750 equipment was used to examine H<sub>2</sub>-TPR, O<sub>2</sub>-TPO, and NH<sub>3</sub>-TPD analyses with an automated system attached by ChemiSoft TPx software.

### 2.3. Photo-electrochemical measurements

The cyclic voltammetry (CV), chronoamperometry (CA), and electrochemical impedance spectroscopy (EIS) electrochemical analyses of the catalysts were performed using CHI 660 and 601 E potentiostat devices to examine activity, stability, and resistance, respectively. All analyses were performed in a three-electrode system with a reference

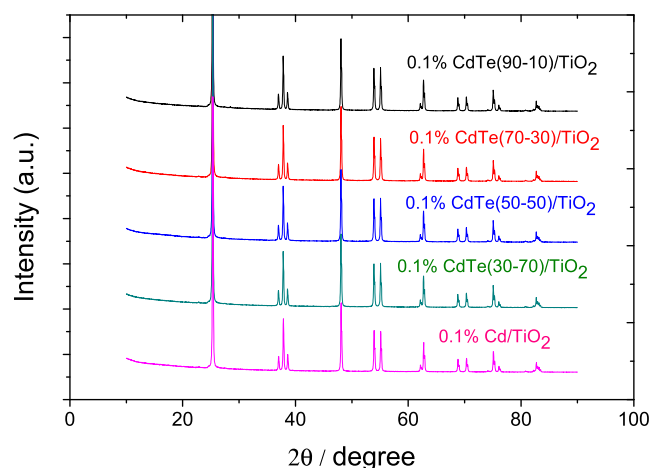


**Fig. 1.** XRD patterns of 0.1% Cd/TiO<sub>2</sub> and 0.1% CdTe/TiO<sub>2</sub> catalysts.

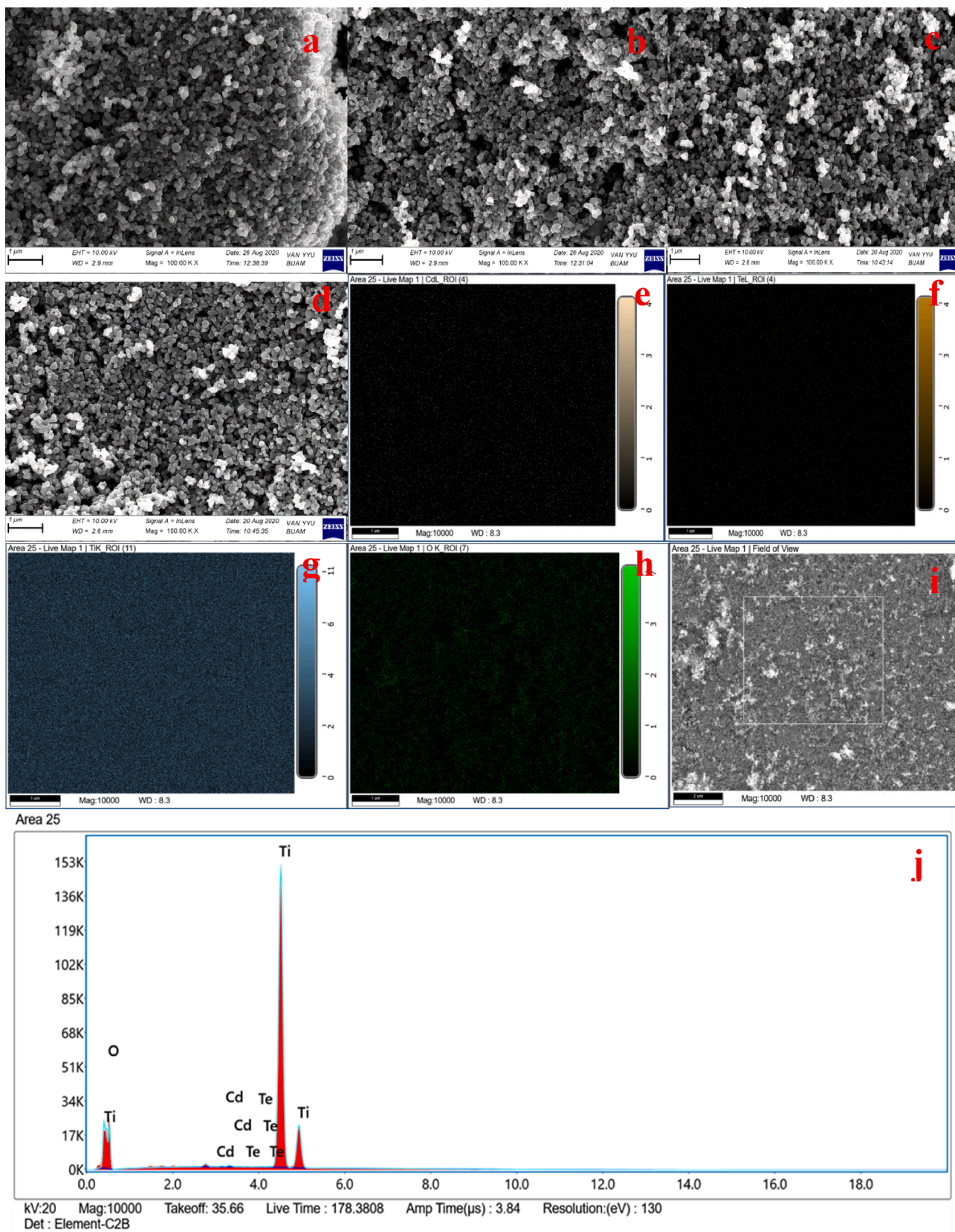
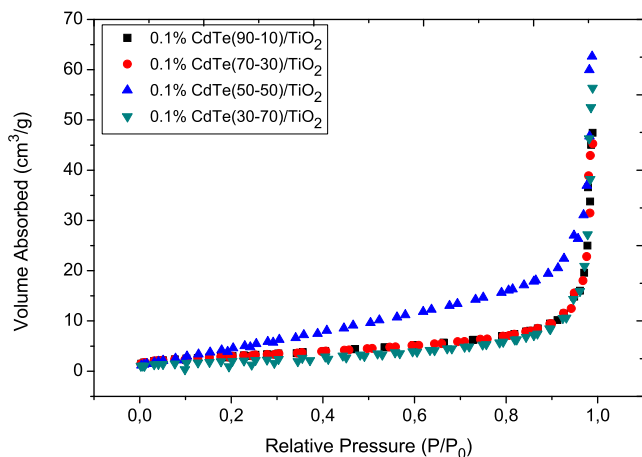


Fig. 2. SEM-EDX and mapping images (Cd (e), Te (f), Ti (g), O (h)) of 0.1% CdTe(50–50)/TiO<sub>2</sub> (a–d, i, j) catalyst.

**Table 2**  
The weight elemental composition of 0.1% CdTe/TiO<sub>2</sub> catalysts.

Elements (%)	Samples			
	0.1 % CdTe (90–10)/TiO <sub>2</sub>	0.1 % CdTe (70–30)/TiO <sub>2</sub>	0.1 % CdTe (50–50)/TiO <sub>2</sub>	0.1 % CdTe (30–70)/TiO <sub>2</sub>
Cd	0.22	0.16	0.13	0.08
Te	0.03	0.07	0.03	0.05
Ti	68.11	75.08	71.17	69.14
O	31.64	24.69	28.67	30.73



**Fig. 3.** N<sub>2</sub> adsorption–desorption isotherms of CdTe/TiO<sub>2</sub> catalysts.

electrode (Ag/AgCl, 3 M KCl), working electrode (Titanium metal), and counter electrode (Pt wire, L × diameter 50 cm × 0.2 mm) in 1 M KOH (>85 %) and 1 M KOH + 0.5 M glucose (≥99.5 %) solution. The catalyst slurry was obtained from mixing CdTe/TiO<sub>2</sub> catalysts and Nafion and it was transferred over titanium metal having 0.5 cm<sup>2</sup> area. The CV, CA, and EIS analyses were used to investigate catalytic activities of photocatalytic glucose electrooxidation at dark and under UV illumination. The UV lamp used for illumination had a power of 366 nm (long wavelength) and 6 W in a cabinet connected to the UVP device.

### 3. Results and discussion

**Fig. 1** illustrates the XRD patterns of Cd/TiO<sub>2</sub> and CdTe/TiO<sub>2</sub> catalysts. The diffraction peaks at around 2θ of 25.32°, 36.92°, 37.48°, 47.98°, 53.91°, 55.19°, 62.67°, 68.85°, 70.40°, 75.04°, 76.07°, and 82.77° correspond to (1 0 1), (1 0 3), (0 0 4), (1 1 2), (2 0 0), (1 0 5), (2 1 1), (2 0 4), (1 1 6), (2 2 0), (2 1 5), and (2 2 4), crystal planes of TiO<sub>2</sub> anatase, respectively (JCPDS: 21-1272) [44]. All the diffraction peaks in the XRD models were appeared to describe well the TiO<sub>2</sub> anatase phase. However, there were no characteristic peaks of CdTe due to the low metal amount in CdTe/TiO<sub>2</sub> catalysts [45]. Huang et al [46] reported the crystal structural properties of CdS-doped TiO<sub>2</sub> by XRD analysis and reported that no peak was formed due to the low amount of CdS and dispersed well into the TiO<sub>2</sub>. The crystalline size of 0.1 % CdTe(90–10)/TiO<sub>2</sub>, 0.1 % CdTe(70–30)/TiO<sub>2</sub>, 0.1 % CdTe(50–50)/TiO<sub>2</sub>, and 0.1 % CdTe(30–70)/TiO<sub>2</sub> catalysts were calculated by utilizing Scherrer equation and found to be 51.9, 51.6, 52.2, and 52.1 nm, respectively.

The SEM-EDX and mapping analyses were realized to observe the surface morphology of the CdTe(50–50)/TiO<sub>2</sub> catalyst. **Fig. 2(a–d)** shows SEM images (1 μm) of the catalyst. Due to the low amount of metal used during the synthesis compared to TiO<sub>2</sub>, SEM images mostly showed TiO<sub>2</sub> structures. This shows that the metals are not agglomerate and are well dispersed. Cd, Te, Ti, and O structures were demonstrated to be formed in EDX and mapping analysis. According to the EDX analysis results, the presence of Cd and Te was observed in all CdTe/TiO<sub>2</sub> catalysts (**Table 2**

**Table 3**  
BET surface area, pore-volume, pore size, and nanoparticle size analysis for 0.1% CdTe/TiO<sub>2</sub> catalysts.

Catalyst	BET Surface Area (m <sup>2</sup> /g)	Pore Volume (cm <sup>3</sup> /g)	Pore Size (nm)	Nanoparticle Size (nm)
0.1 % CdTe (90–10)/TiO <sub>2</sub>	7.88	0.073	26.49	761.19
0.1 % CdTe (70–30)/TiO <sub>2</sub>	7.64	0.069	26.33	784.99
0.1 % CdTe (50–50)/TiO <sub>2</sub>	18.04	0.095	14.32	332.60
0.1 % CdTe (30–70)/TiO <sub>2</sub>	6.26	0.087	38.79	958.03

and **Fig. 2j**). It could be seen from **Table 2** and **Fig. 2j**, it was observed that Cd and Te metals were composed of different ratios in the EDX analysis. In addition, the formation of the CdTe/TiO<sub>2</sub> catalyst was illustrated via mapping analysis in which purple, brown, turquoise, and green particles were formed which show the presence of Cd, Te, Ti, and O, respectively (**Fig. 2e–i**).

The N<sub>2</sub> adsorption–desorption isotherms of 0.1 % CdTe/TiO<sub>2</sub> catalysts were given in **Fig. 3** and **Table 3**. It could be observed in **Fig. 3** that the catalysts have a type III adsorption isotherm [47]. The effect of the surface area of the catalysts on the catalytic performance is significant. It was found that the specific surface areas of CdTe/TiO<sub>2</sub> catalysts obtained were in the order of CdTe(50–50)/TiO<sub>2</sub> > CdTe(90–10)/TiO<sub>2</sub> > CdTe(70–30)/TiO<sub>2</sub> > CdTe(30–70)/TiO<sub>2</sub>. CdTe(50–50)/TiO<sub>2</sub> catalyst had the highest surface area and lowest pore and nanoparticle size. This suggests that the increased photocatalytic activity is attributed to a higher surface area of the catalyst and smaller size CdTe particles [48,49].

According to the results of the ICP-MS analysis, the molar atomic ratio of 0.1 % CdTe(90–10)/TiO<sub>2</sub>, 0.1 % CdTe(70–30)/TiO<sub>2</sub>, 0.1 % CdTe(50–50)/TiO<sub>2</sub>, and 0.1 % CdTe(30–70)/TiO<sub>2</sub> catalysts was found to be (95–5), (62–38), (49–51), and (45–55), respectively. In SEM-EDX ve XPS analyses, the molar atomic ratios of 0.1 % CdTe(50–50)/TiO<sub>2</sub> catalyst taken from a certain point were (79–21) and (39–61), respectively. Since these results were taken from a specific point, they were far from ICP-MS results. The ICP-MS results showed that the catalysts were very close to the desired atomic ratios. **Fig. 4** demonstrates the TEM images of 0.1 % CdTe(50–50)/TiO<sub>2</sub> catalyst. In addition, EDX analysis and particle size distribution were performed on the catalyst. It could be shown from **Fig. 4(a–i)**, the particles didn't form agglomeration and were generally homogeneously dispersed. TiO<sub>2</sub> structures indicate the larger particle size, while CdTe metal particles have distributed and smaller particle sizes [50]. The histogram and particle size of the 20 nm image were given in **Fig. 4j** and **k**. Particle size was found as about 1.8 nm. Many studies reported that it was emphasized that the activity increased with the reduction of particle size [51,52]. EDX results revealed the presence of Cd, Te, and TiO<sub>2</sub> particles. This result is equivalent to the SEM-EDX results. Furthermore, **Fig. 5(a–j)** demonstrates the HR-TEM (a–c) and STEM and mapping (d–j) of 0.1 % CdTe(50–50)/TiO<sub>2</sub> catalyst. From **Fig. 5(e–j)**, the presence of Cd, Te, Ti, and O was observed as obtained in the SEM-EDX and mapping results. Furthermore, the formation of the CdTe/TiO<sub>2</sub> catalyst was shown by mapping analysis in which blue, red, pink and/or purple, and green particles were formed which show the presence of Cd, Te, Ti, and O, respectively (**Fig. 5f–j**). Although Ti and O structures were more intense, it was obvious that Cd and Te structures were homogeneously distributed.

The optical properties, one of the most important parameters for the photocatalytic activity of the TiO<sub>2</sub>, Cd/TiO<sub>2</sub>, and CdTe/TiO<sub>2</sub> catalysts were characterized utilizing a UV–visible diffuse reflectance spectrum (UV–vis DRS) in the region of 300–800 nm. **Fig. 6a** and **b** indicate the

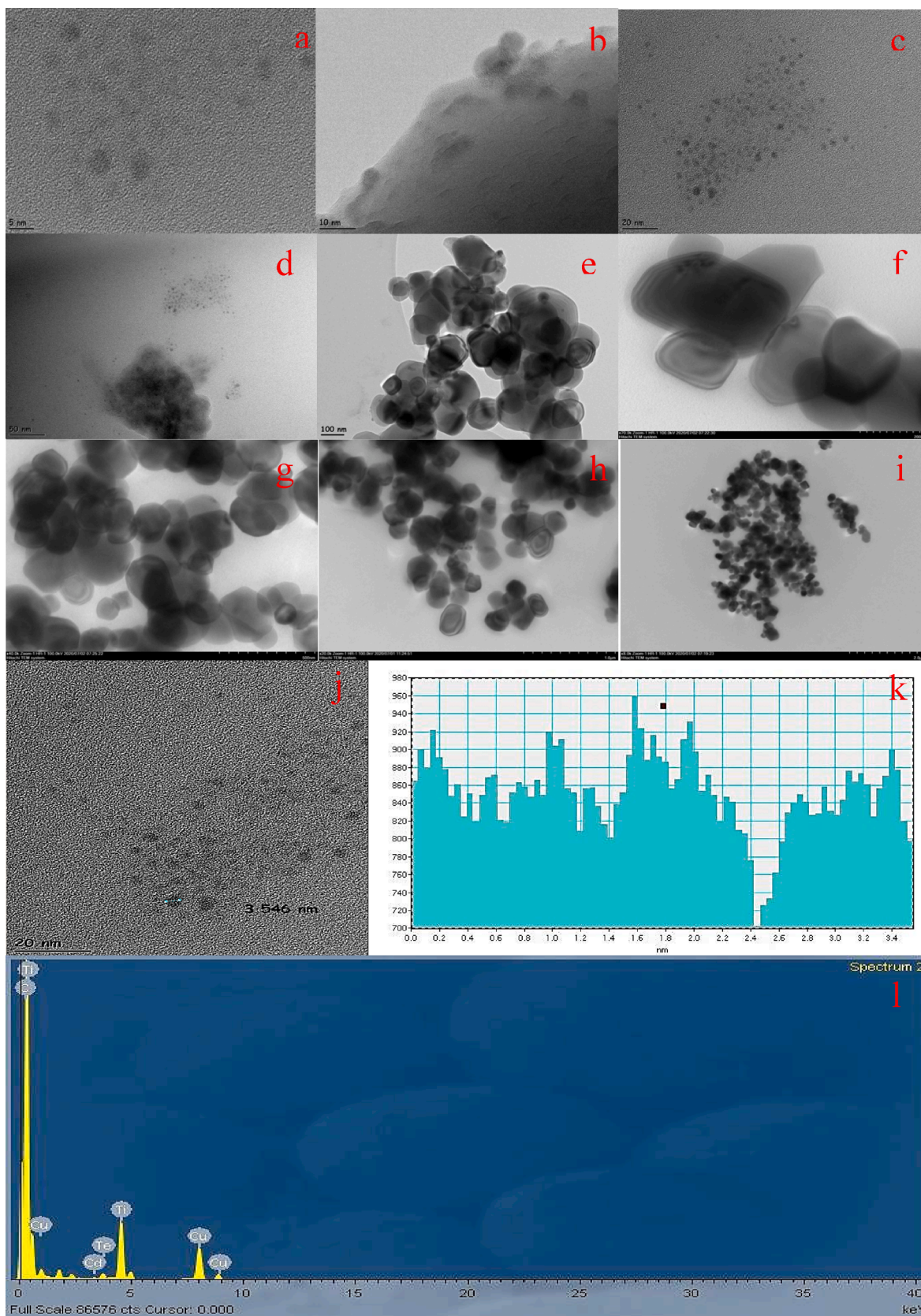


Fig. 4. TEM images of 0.1 % CdTe(50–50)/TiO<sub>2</sub> catalyst (a) 5 nm, (b) 10 nm, (c) 20 nm, (d) 50 nm, (e) 100 nm, (f) 200 nm, (g) 500 nm, (h) 1 μm, (i) 2 μm, (j) and (k) 20 nm particle size histogram with related particle size distribution, and (l) EDX analysis.

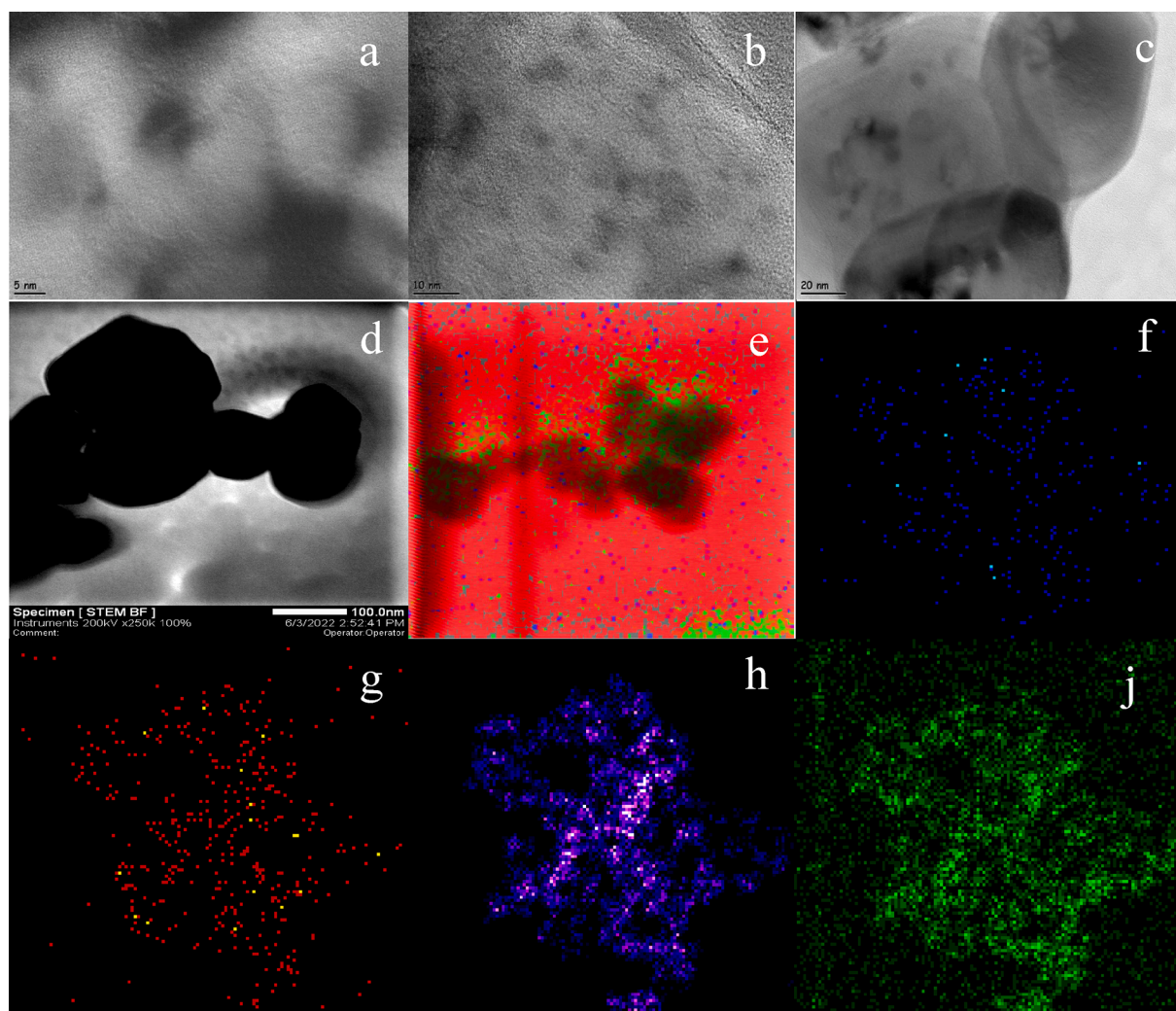


Fig. 5. (a-c) HR-TEM and (d) STEM and EDS elemental mapping (mix (e), Cd (f), Te (g), Ti (h), O (j)) of 0.1% CdTe(50-50)/TiO<sub>2</sub> catalyst.

UV-vis DRS and the Tauc plots, respectively. As depicted in Fig. 6a, TiO<sub>2</sub> displayed a strong absorption under ultraviolet light with a wavelength at about 400 nm due to its band-gap of anatase-TiO<sub>2</sub>. The preparation of TiO<sub>2</sub> with Cd and CdTe metals was aimed to change the band-gap but remain in the UV region and increase the catalytic activity. Fig. 6a illustrates that the absorption spectrum of Cd/TiO<sub>2</sub> and CdTe/TiO<sub>2</sub> is stretched from 400 nm to 407 and 410 nm, respectively. As shown from Tauc plots in Fig. 7b, the bandgap energies of the TiO<sub>2</sub>, Cd/TiO<sub>2</sub>, and CdTe/TiO<sub>2</sub> catalysts obtained from the formula  $\lambda = 1240/E_g$  are 3.25 eV, 3.22, and 3.15 eV, respectively. These band-gap results show that the introduction of Cd and CdTe into the TiO<sub>2</sub> structure results in the increase of the ability for light absorption [53]. Furthermore, the addition of CdTe into TiO<sub>2</sub> shows that it can effectively improve the absorption of UV light for catalytic activity. Optical band gap values (E<sub>g</sub>) of TiO<sub>2</sub>, 0.1 % Cd/TiO<sub>2</sub>, and 0.1 %CdTe(50-50)/TiO<sub>2</sub> catalysts were found from measured UV-vis DRS using Tauc plot (Fig. 6). The conduction band minimum (E<sub>CB</sub>) and valence band maximum (E<sub>VB</sub>) of a semiconductor can be calculated by an empirical equation [54]:

$$E_{VB} = \chi - E^e + E_g/2$$

$$E_{CB} = E_{VB} - E_g$$

where  $\chi$  is the electronegativity of the semiconductor (5.81 eV); E<sup>e</sup> is the energy of free electrons on the hydrogen scale (4.5 eV). The extracted band edge positions and band gaps of catalysts were given in Fig. 6c. As can be seen in Fig. 6c and 6d, the CdTe/TiO<sub>2</sub> heterostructure catalyst has

a Schottky-junction charge transfer mechanism [55]. The Schottky-junction, which enables efficient separation of photogenerated electrons and supports photocatalytic activity, electrons can be transferred from the photocatalyst to the co-catalyst via the aligned Fermi level. Thus, it leads to spatial charge separation where positive charges accumulate on the semiconductor and negative charges accumulate on the co-catalyst [56].

The CdTe/TiO<sub>2</sub> catalysts were examined by using glucose as fuel to the photocatalytic performance. The CV analysis was realized to investigate the catalytic activity, stability, and resistance of catalysts, respectively. These analyzes were obtained in the dark and under UV illumination in 1 M KOH + 0.5 M glucose solution. Fig. 7(a-d) shows the photocatalytic glucose electrooxidation in dark and under UV illumination of catalysts. The electrochemical behaviors of 0.1 % CdTe/TiO<sub>2</sub> catalysts were performed by CV analysis at between -0.65 and 0.65 V potential a scan rate of 100 mV s<sup>-1</sup> in 1 M KOH and 1 M KOH + 0.5 M glucose solution (Fig. 7a, b). Table 4 summarizes the catalytic activities of the CdTe/TiO<sub>2</sub> catalysts formed at the total current values in the KOH and glucose solution. Although glucose has a high energy density, it is a difficult fuel to break down. Therefore, the catalysts were evaluated over the total current because oxidation peaks did not occur in glucose electrooxidation measurements. It could be shown from Fig. 7b that the 0.1 % CdTe(50-50)/TiO<sub>2</sub> catalyst exhibited the best catalytic activity compared to the others, with specific activity at the total current (glucose) of 6.22 mA cm<sup>-2</sup> (15583.50 mA mg<sup>-1</sup>Cd) in the dark. Fig. 7c indicates a comparison of 0.1 % CdTe(50-50)/TiO<sub>2</sub> catalyst in the dark

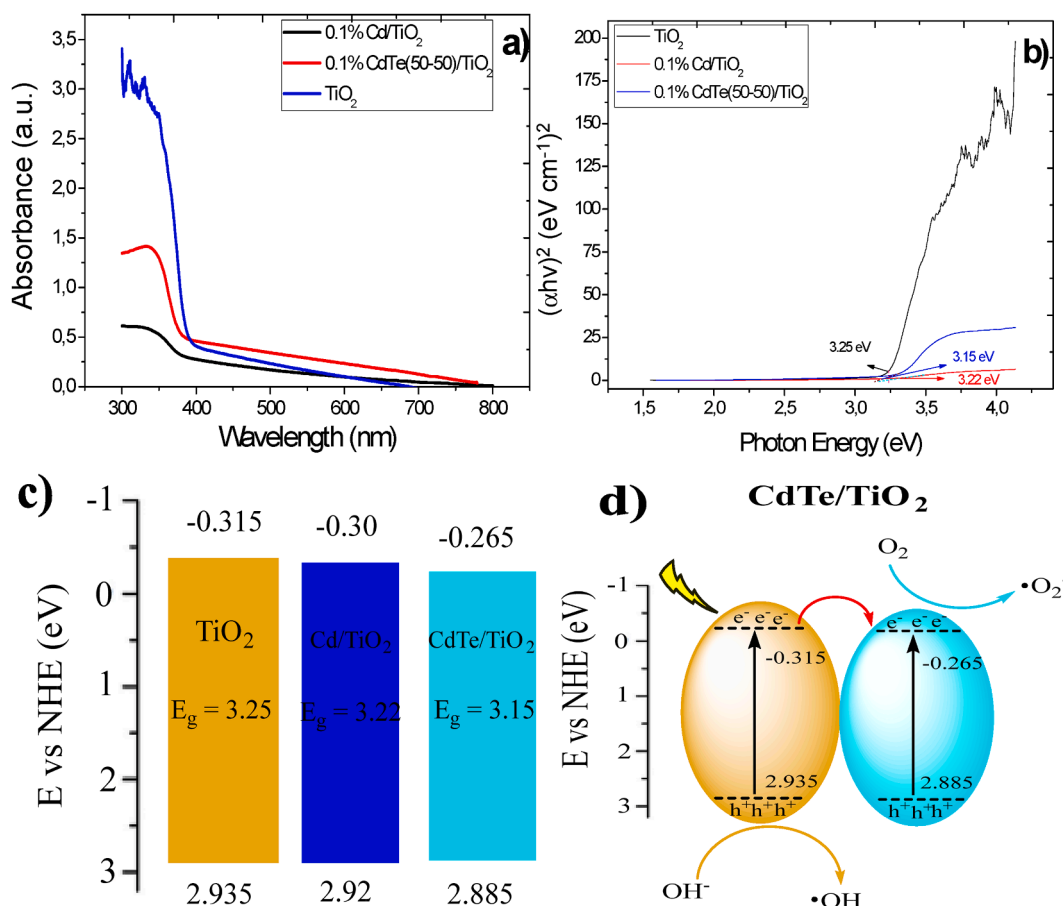
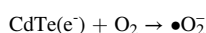
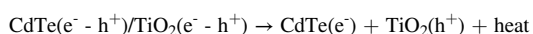
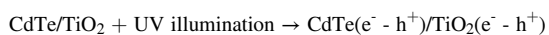


**Fig. 6.** (a) UV-vis DRS, (b) Tauc plots, (c) Schematic diagram of band edge alignment of the TiO<sub>2</sub>, 0.1% Cd/TiO<sub>2</sub>, and 0.1% CdTe(50–50)/TiO<sub>2</sub> catalysts, and (d) Schematic illustration of the proposed reaction mechanism for photo-electrochemical oxidation by CdTe/TiO<sub>2</sub> photocatalyst under UV illumination.

with 1 M KOH and 1 M KOH + 0.5 M glucose. The 6.22 mA cm<sup>-2</sup> specific activity occurring in the total current is the catalytic activity originating from glucose. The 0.1 % CdTe(50–50)/TiO<sub>2</sub> catalyst were examined under UV illumination for the photocatalytic glucose electrooxidation (Fig. 7d). The 0.1 % CdTe(50–50)/TiO<sub>2</sub> catalyst exhibited approximately 2.7 time better catalytic activity with an onset potential of –0.36 V (Ag/AgCl) and specific activity of 16.68 mA cm<sup>-2</sup> (41798.85 mA mg<sup>-1</sup>Cd) under UV illumination according to dark. The low onset potential prevents charge recombination and lowers the kinetic barrier [57]. It also showed better photocatalytic activity under UV illumination compared to C-TNT (9.10 mA cm<sup>-2</sup>) (see Table 1) and 0.1 % Cd/TiO<sub>2</sub> (6.00 mA cm<sup>-2</sup>) (see Table 1) and 0.1 % Te/TiO<sub>2</sub> (2.86 mA cm<sup>-2</sup>), 0.1 % CdO/TiO<sub>2</sub> (2.20 mA cm<sup>-2</sup>), and 0.1 % TeO<sub>3</sub>/TiO<sub>2</sub> (1.80 mA cm<sup>-2</sup>) catalysts (Fig. 8a). CdTe-TiO<sub>2</sub> photocatalyst has been investigated for applications such as photocatalytic degradation [58], photogenerated cathodic protection [59], and solar cells [60] the literature. It has been reported that CdTe-TiO<sub>2</sub> photocatalyst is a highly efficient material in photocatalytic systems. The stability of the 0.1 % CdTe(50–50)/TiO<sub>2</sub> catalyst was examined during 20 cycles by CV analysis (Fig. 8b). It was observed that although there was a rapid decrease during the first 5 cycles, afterward it gradually stabilized. Although it contains a small amount of metal compared to the literature, it can be a promising photoanode for photoelectrochemical fuel cells with its high specific and mass activity. The major involved reactions can be summarized as follows:



The CdTe/TiO<sub>2</sub> catalyst was examined by H<sub>2</sub>-TPR analysis to investigate the behavior during the reduction with hydrogen and the analysis results were shown in Fig. 9a. H<sub>2</sub>-TPR analysis can provide information about the interaction between CdTe and TiO<sub>2</sub> due to the effects on the catalytic performance and properties of the catalyst when TiO<sub>2</sub> interacts with the metal [61]. TiO<sub>2</sub> and 0.1 % Cd/TiO<sub>2</sub> catalysts were performed TPR, TPO, and TPD analyzes in our previous study[33]. TPR profiles show the reduction behavior of metal oxides of catalysts performed under the same operating conditions. The H<sub>2</sub>-TPR analysis of TiO<sub>2</sub> examined by many researchers in the literature can be attributed to the peak TiO<sub>2</sub> or Ti<sup>4+</sup> reduction obtained at approximately 400–750 °C [62]. When TiO<sub>2</sub> is doped with Cd or CdTe metals, its reducibility increases, and therefore the reduction temperatures decrease. The O<sub>2</sub>-TPO analysis of 0.1 % CdTe(50–50)/TiO<sub>2</sub> catalyst was demonstrated in Fig. 9b. TPO analysis is a material characterization process that is heated to a certain temperature by passing an oxidizing gas mixture containing oxygen on the sample and then can form oxidation in the thermal excitation that occurs. It could be seen from Fig. 9b that TiO<sub>2</sub>, 0.1 % Cd/TiO<sub>2</sub>, and 0.1 % CdTe(50–50)/TiO<sub>2</sub> catalysts have sharp peak TPO profiles at 785 °C, 320 °C, and 475 °C, respectively. When it was doped with Cd and Te metals, it was seen that the metals are oxidized before the support material and the oxidation temperature decreases due to the metal support contact [63]. In addition, the higher oxidation temperature of the CdTe/TiO<sub>2</sub> catalyst compared to Cd/TiO<sub>2</sub> can be due to the formation of Cd and Te alloys. TPD analysis is used to characterize the adsorption sites on the sample with an inert gas mixture of gases such as NH<sub>3</sub> and CO<sub>2</sub>, which examines the events occurring on the surface of solid samples and

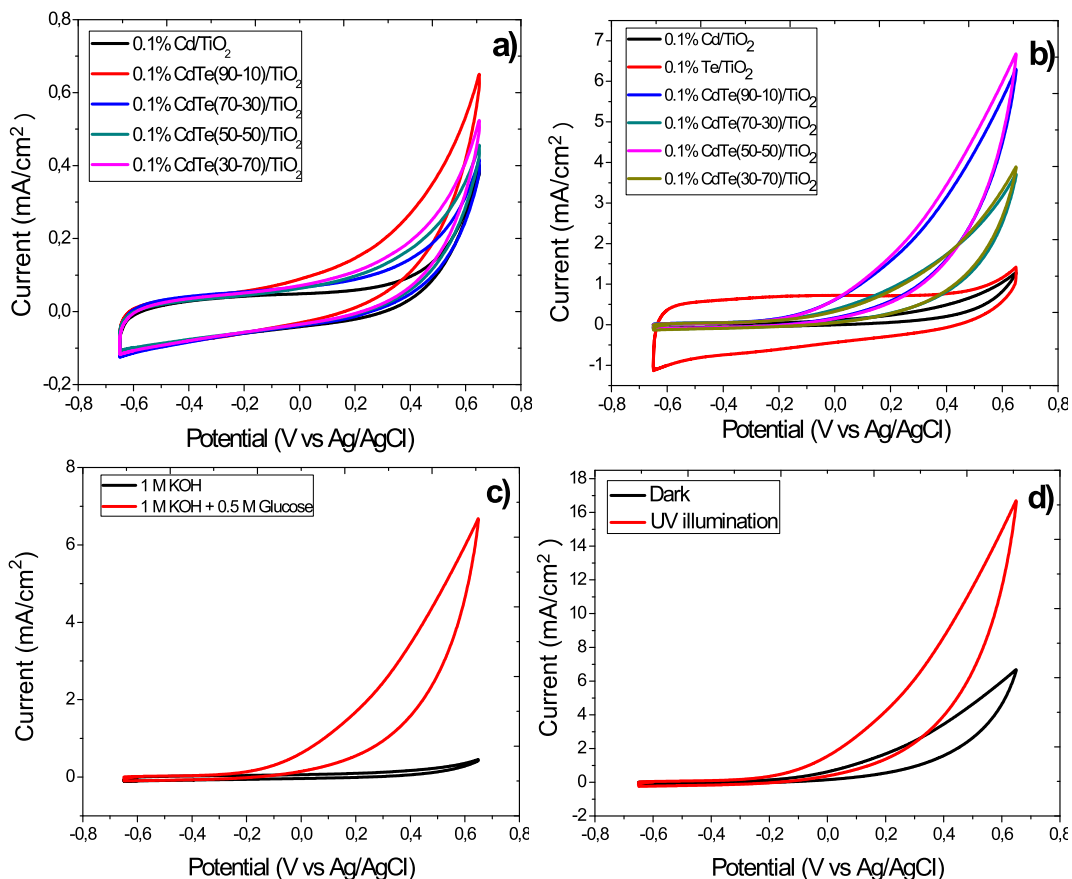


Fig. 7. Cyclic voltammograms of 0.1 % CdTe/TiO<sub>2</sub> catalysts in (a) 1 M KOH, (b) 1 M KOH + 0.5 M glucose, (c) comparison KOH and glucose of 0.1 % CdTe(50–50)/TiO<sub>2</sub> catalyst, (d) dark and under UV illumination of 0.1 % CdTe(50–50)/TiO<sub>2</sub> catalyst at 100 mV/s scan rate.

**Table 4**  
The electrochemical behaviors of 0.1% CdTe/TiO<sub>2</sub> catalysts in dark for glucose electrooxidation.

Sample	Total Current (KOH, mA/cm <sup>2</sup> )	Total current (Glucose, mA/cm <sup>2</sup> )	Total Current (Normal, mA/cm <sup>2</sup> )	Mass Activity (mA/mg Cd)	Onset Potential (V)
0.1 % Cd/TiO <sub>2</sub>	0.40	1.29	0.89	2227.23	-0.24
0.1 % CdTe(90–10)/TiO <sub>2</sub>	0.65	6.26	5.61	14040.80	-0.29
0.1 % CdTe(70–30)/TiO <sub>2</sub>	0.41	3.69	3.28	8212.32	-0.29
0.1 % CdTe(50–50)/TiO <sub>2</sub>	0.45	6.67	6.22	15583.50	-0.27
0.1 % CdTe(30–70)/TiO <sub>2</sub>	0.52	3.86	3.34	8380.59	-0.27

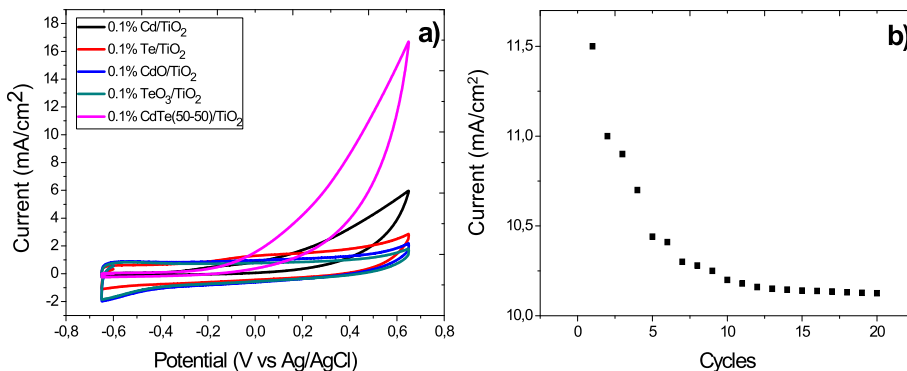


Fig. 8. Cyclic voltammograms of (a) 0.1 % Cd/TiO<sub>2</sub> [33], 0.1 % Te/TiO<sub>2</sub>, 0.1 % CdO/TiO<sub>2</sub>, 0.1 % TeO<sub>3</sub>/TiO<sub>2</sub>, and 0.1 % CdTe(50–50)/TiO<sub>2</sub> catalysts (b) stability of 0.1 % CdTe(50–50)/TiO<sub>2</sub> catalyst under UV illumination at 100 mV/s scan rate in 1 M KOH + 0.5 M glucose solution.

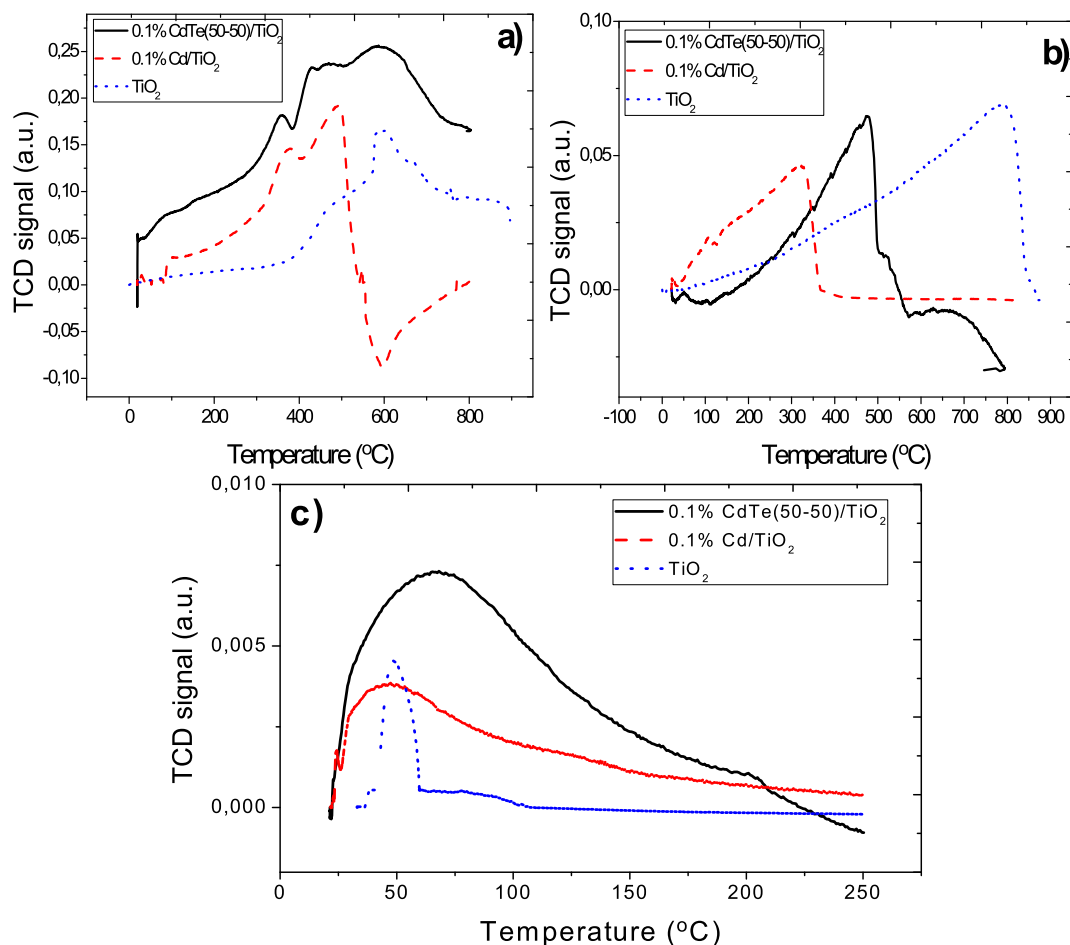


Fig. 9. H<sub>2</sub>-TPR a), O<sub>2</sub>-TPO b), and NH<sub>3</sub>-TPD c) profiles of 0.1% CdTe(50–50)/TiO<sub>2</sub> catalyst.

whose temperature is changed by a temperature program. This analysis primarily involves measuring the rate of adsorption from the sample surface at low temperatures with a known gas and inert gas mixture, and the rate of desorption as the temperature increases [64]. The NH<sub>3</sub>-TPD curves of TiO<sub>2</sub>, 0.1 % Cd/TiO<sub>2</sub>, and 0.1 % CdTe(50–50)/TiO<sub>2</sub> catalysts were illustrated in Fig. 9c. TPD curves change the acidic state of the sample as a weak acid, medium acid, and strong acid as the temperature increases [65,66]. While the peaks assigned to physical adsorption for TiO<sub>2</sub> and Cd/TiO<sub>2</sub> catalysts were found at about 50 °C, it was obtained at about 70 °C for CdTe/TiO<sub>2</sub>. It was observed that the peak area increases when TiO<sub>2</sub> was doped with metal. Furthermore, CdTe/TiO<sub>2</sub> catalyst obtained NH<sub>3</sub> desorption peak close to weak acid regions (100–150 °C).

Fig. 10(a–e) illustrates the possible chemical states of Cd and Te in the 0.1 % CdTe(50–50)/TiO<sub>2</sub> catalyst defined by using XPS analysis. In all XPS results, peak positions were determined relative to C 1s at a binding energy of 284.6 eV. The general spectrum of XPS analysis (Fig. 10a) of 0.1 % CdTe(50–50)/TiO<sub>2</sub> catalyst demonstrates peaks C 1s, Ti 2p, O 1s, Cd 3d, and Te 3d. The C 1s of three different chemical shifts components with the binding energy of 284.6, 286.1, and 288.0 eV could be attributed to C–C or C=C, C–O or C–OH, and C=O [67,68]. It could be seen from Fig. 10c, the Ti 2p spectrums at binding energy about 459.1 eV and 464.8 eV were composed in Ti 2p<sub>3/2</sub> and Ti 2p<sub>1/2</sub>. The binding energy difference between Ti 2p<sub>3/2</sub> and Ti 2p<sub>1/2</sub> was 5.7 eV, showing a normal state of Ti<sup>4+</sup> consisted [69]. The binding energy at 405.5 eV and 412.1 eV of Cd 3d (Fig. 10d) have two peaks at 3d<sub>5/2</sub> and 3d<sub>3/2</sub>, which shows the possible formation of CdO which are consistent with the values noticed for Cd<sup>2+</sup> [53,70]. Fig. 10e shows the binding energies of Te 3d. The binding energy at 583.0 eV occurred from the exposed CdTe bond. The binding energies at 576.3 eV and 586.4 eV

corresponded to Te 3d<sub>5/2</sub> and Te 3d<sub>3/2</sub> at the Te–O bond formation peak from oxidation of Te<sup>4+</sup> species. In addition, the corresponding peak at 578.6 eV of Te 3d indicates the possible formation in particular TeO<sub>3</sub> [71]. Furthermore, the measured atomic concentrations and probable chemical states of C 1s, Ti 2p, O 1s, Cd 3d, and Te 3d for the 0.1 % CdTe(50–50)/TiO<sub>2</sub> catalyst are summarized in Table 5. When the oxygen in Te–O and Cd–O bonds was calcined at 400 °C under argon gas, it can be concluded that there are some TeO<sub>2</sub>, TeO<sub>3</sub>, and CdO formed by oxidation of CdTe.

Fig. 11 demonstrates the fluorescence spectrum of TiO<sub>2</sub> and 0.1 % CdTe(50–50)/TiO<sub>2</sub> catalysts. Thanks to this spectrum, the photocatalytic activity efficiency of the catalysts and the charge capturing properties in the semiconductor could be determined [83]. It could be seen from Fig. 11 that the peak density of 0.1 % CdTe(50–50)/TiO<sub>2</sub> catalyst at about 362 nm, 376 nm, and 421 nm was weaker than TiO<sub>2</sub>. Fluorescence emission in semiconductor materials is mainly due to the recombination of photo-induced electrons and holes [84]. Thus, the 0.1 % CdTe(50–50)/TiO<sub>2</sub> catalyst could effectively divide photo-induced electrons from the holes on the TiO<sub>2</sub> surface, therefore making their recombination difficult and resulting in increased photocatalytic activity.

CA analysis was performed to measure the stability and poison resistance of CdTe/TiO<sub>2</sub> catalysts. Fig. 12(a–d) shows the CA curves of catalysts. CA analysis of 0.1 % CdTe(50–50)/TiO<sub>2</sub> catalyst were performed at different potentials (0.1 V, 0.3, and 0.6 V) under UV illumination (Fig. 12a). CA analysis at 0.6 V potential exhibited the best resistance and stability. After 1000 s, 0.1 % CdTe(50–50)/TiO<sub>2</sub> catalyst was better activity and stability with 2.25 mA cm<sup>–2</sup> specific activity compared to other catalysts under UV illumination at 0.6 V potential

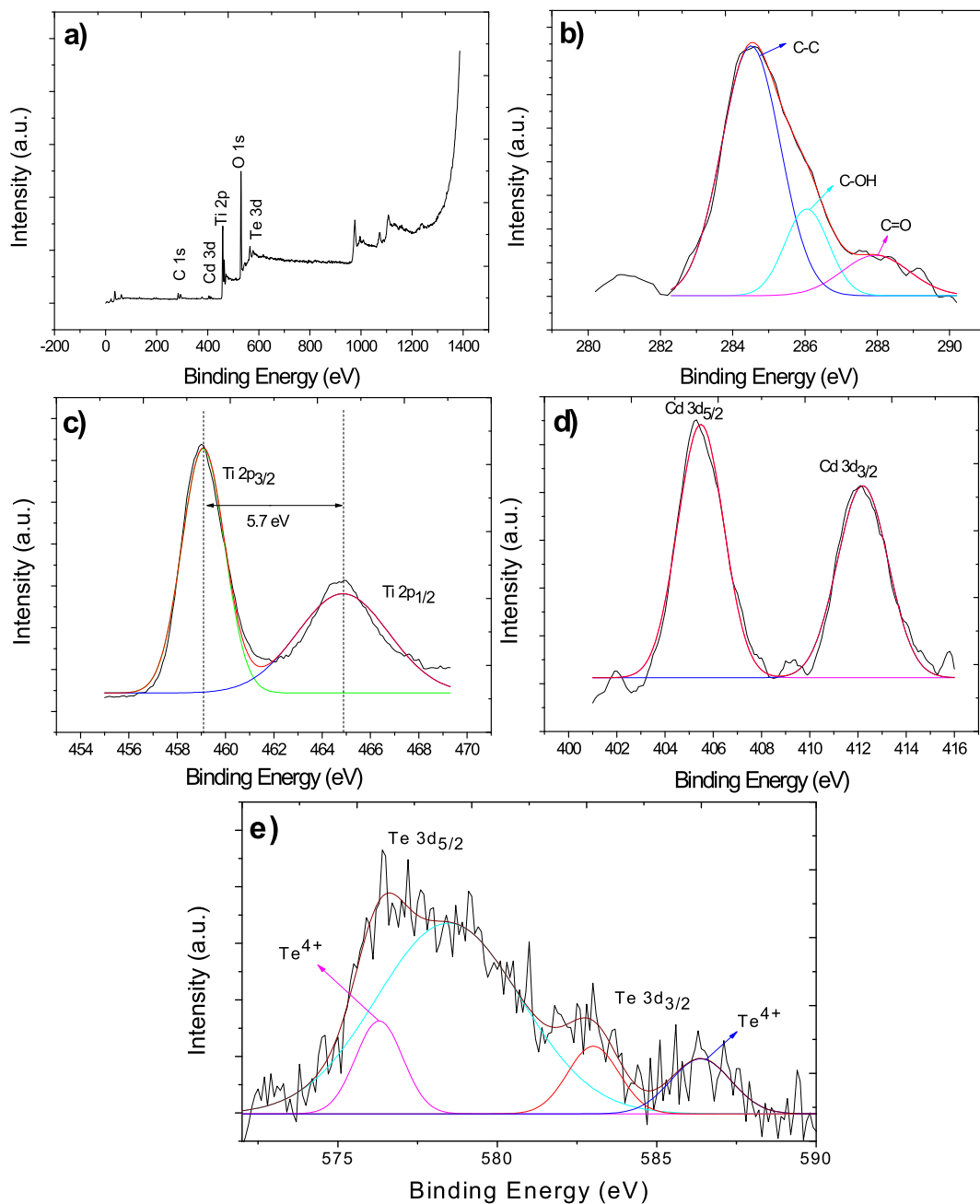


Fig. 10. XPS spectra of (a) general spectrum (b) C 1s, (c) Ti 2p, (d) Cd 3d, (e) Te 3d for 0.1 % CdTe(50-50)/TiO<sub>2</sub> catalyst.

**Table 5**

The results of curve fitting and probable chemical states of the XPS spectra of C 1s, Ti 2p, Cd 3d, and Te 3d regions.

Name	Start BE	Peak BE	End BE	FWHM (eV)	Area	At. %	BE (eV)	Possible Chemical State	Relative Intensity %	Reference
C 1s	282.1	284.6	290.1	2.619	1233.2	5.408	284.6	C—C	65.90	[67]
							286.1	C—O	23.08	[72]
							288.0	C=O	11.02	[73]
O 1s	526.2	530.0	538.0	2.665	43909.5	65.719	—	—	—	—
							—	—	—	—
Ti 2p	456.3	459	467.6	1.978	25537.7	21.454	458.7	Ti <sup>4+</sup>	38.82	[74]
							459.5	Ti <sup>3+</sup>	33.36	[75]
							464.9	Ti <sup>4+</sup>	27.82	[76]
Cd 3d <sub>3</sub>	402.4	412.2	415.3	2.461	1481.2	0.541	405.5	Cd <sup>2+</sup>	53.01	[77]
							412.1	Cd <sup>2+</sup>	46.99	[78]
							576.3	TeO <sub>2</sub>	17.66	[79]
Te 3d <sub>5</sub>	573.6	576.4	581.2	4.625	3539.1	0.857	578.6	TeO <sub>3</sub>	52.87	[80]
							583.0	CdTe	13.67	[81]
							586.4	TeO <sub>2</sub>	15.80	[82]
							—	—	—	—

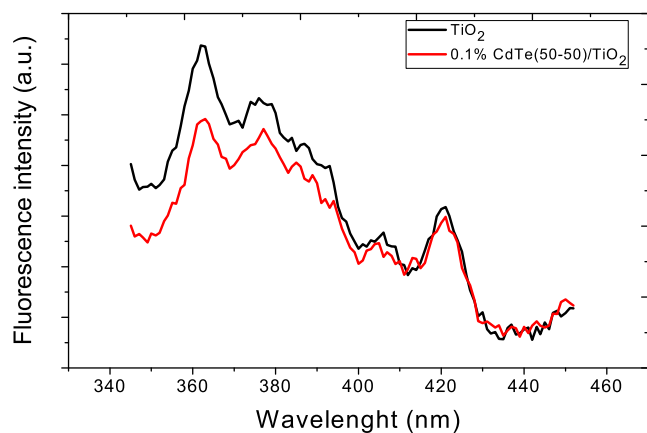


Fig. 11. Fluorescence spectrum of the  $\text{TiO}_2$  and 0.1%  $\text{CdTe}(50-50)/\text{TiO}_2$  catalysts.

(Fig. 12b, d). It could be seen from Fig. 12c that the 0.1 %  $\text{CdTe}(50-50)/\text{TiO}_2$  catalyst taken under UV illumination was about 9 times more stable than received at the dark ( $0.26 \text{ mA cm}^{-2}$ ). As in the CV results, 0.1 %  $\text{CdTe}(50-50)/\text{TiO}_2$  catalyst exhibited the best activity and stability compared to the dark and other catalysts.

Fig. 13(a-c) demonstrates the Nyquist plots obtained from the EIS analysis to examine the electrocatalytic resistance of the 0.1 %  $\text{CdTe}/\text{TiO}_2$  catalysts. These plots are usually known as semicircles, where the electrocatalytic resistance increases as the diameter of the circle decrease [85,86]. The charge transfer resistance ( $R_{ct}$ ) is associated with the diameter of the semicircle because as the diameter decreases,  $R_{ct}$

decreases, and so the catalytic activity increases [87]. Fig. 13a indicates the Nyquist plots of the 0.1 %  $\text{CdTe}(50-50)/\text{TiO}_2$  taken under UV illumination in different potentials (0.1 V, 0.3 V, 0.4 V, 0.5 V, and 0.6 V). As seen in Fig. 13a, the Nyquist plot taken at the potential of 0.6 V exhibited the best photocatalytic activity. It could be clearly seen from Fig. 13b that the  $R_{ct}$  can be listed as follows; 0.1 %  $\text{CdTe}(70-30)/\text{TiO}_2 > 0.1 \text{ % CdTe}(30-70)/\text{TiO}_2 > 0.1 \text{ % CdTe}(90-10)/\text{TiO}_2 > 0.1 \text{ % CdTe}(50-50)/\text{TiO}_2$ . The 0.1 %  $\text{CdTe}(50-50)/\text{TiO}_2$  catalyst has the highest carrier transfer performance because it has the lowest semicircular shape and charge transfer resistance compared to other catalysts. Furthermore, the carrier transfer performance was higher as the  $R_{ct}$  value under UV illumination was lower compared to dark (Fig. 13c). As a result, 0.1 %  $\text{CdTe}(50-50)/\text{TiO}_2$  catalyst indicated the highest photocatalytic activity as in CV and CA results.

#### 4. Conclusion

The impregnation method was used to synthesize  $\text{TiO}_2$  supported CdTe catalysts in different atomic molar (90–10, 70–30, 50–50, and 30–70). The XRD, SEM-EDX, TEM, XPS, UV–vis spectroscopy, Fluorescence spectroscopy, TPR, TPO, and TPD analyzes were realized to characterize the photocatalysts. The XRD results revealed that only anatase- $\text{TiO}_2$  structures were formed because very low amount of CdTe metal was used. This shows that the metals were well dispersed in  $\text{TiO}_2$  [46]. SEM-EDX and mapping and TEM-EDS results demonstrated that anatase- $\text{TiO}_2$  and CdTe metal particles were formed. In addition, it was observed that CdTe particles had a particle size of 1.8 nm and were homogeneously dispersed. The fact that the 0.1 %  $\text{Cd}/\text{TiO}_2$  [88] catalyst in the previous study was lower than the particle size (2.8 nm) indicates increased catalytic activity, as highlighted in most literature studies

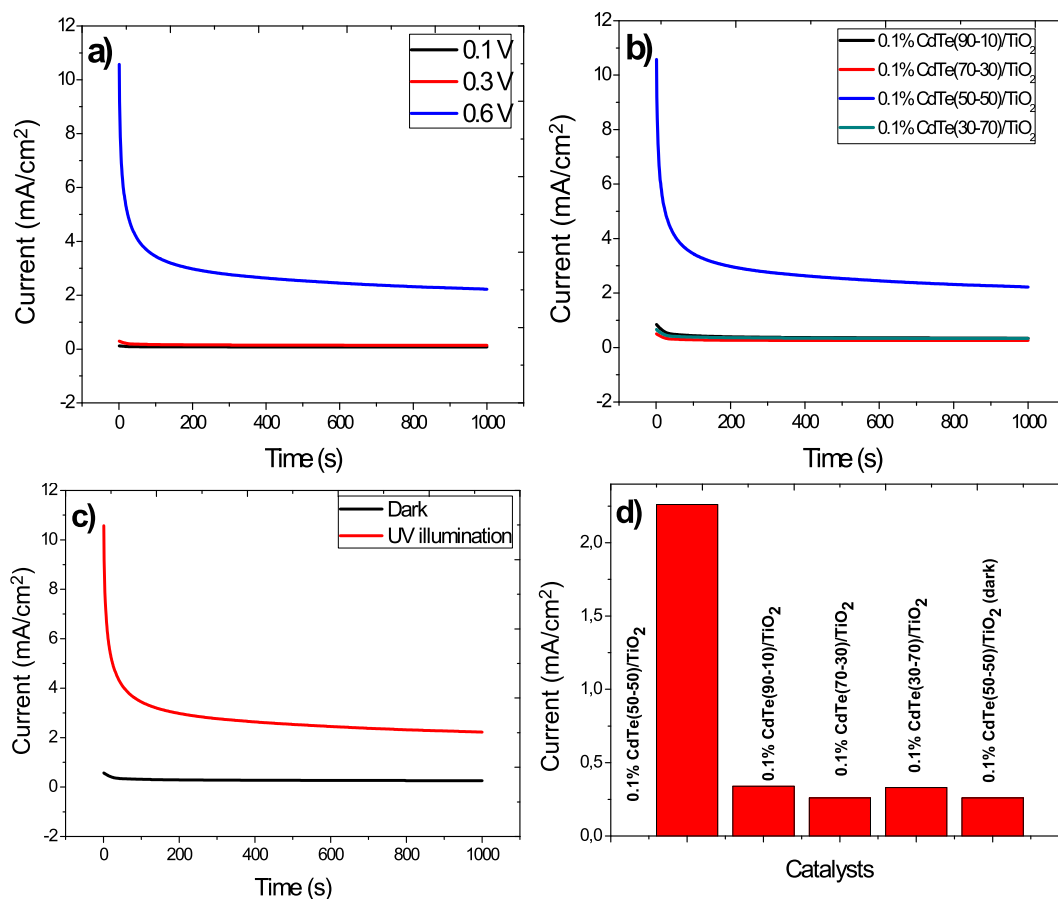
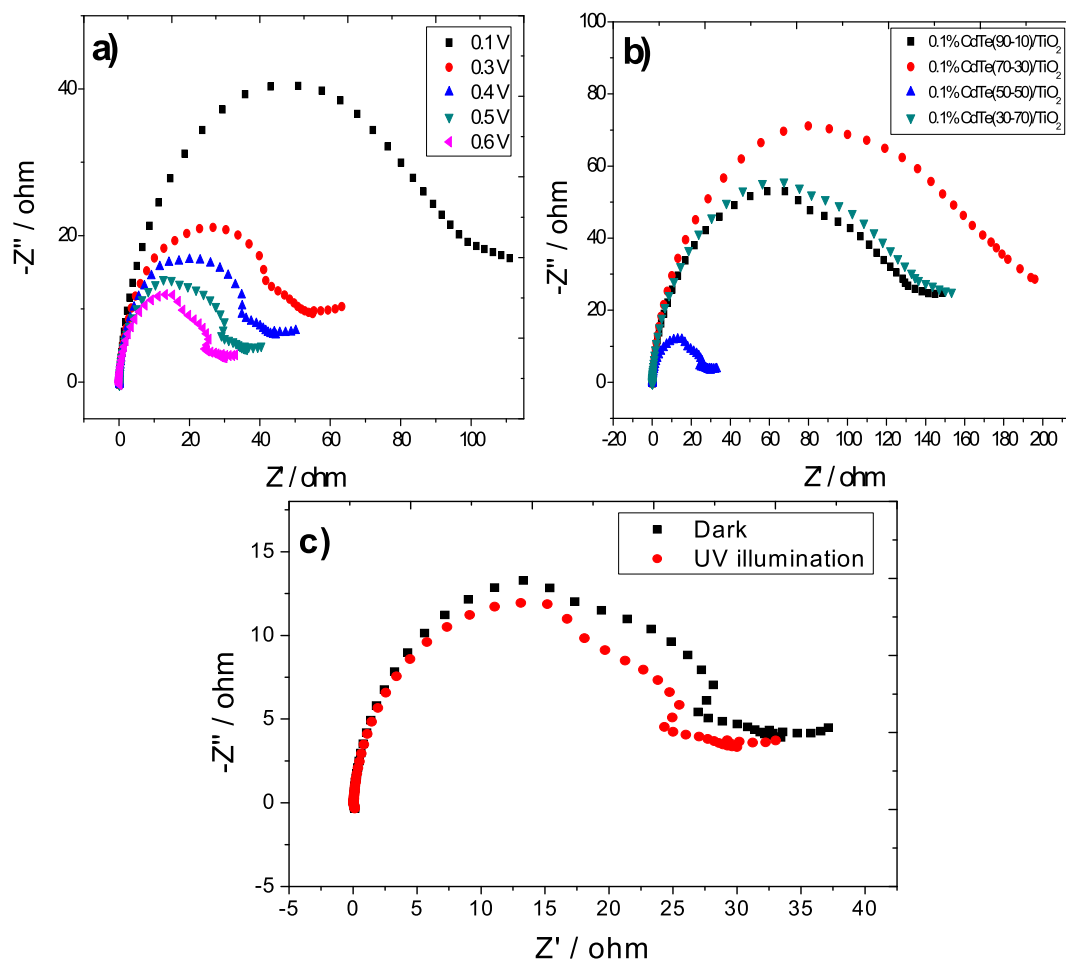


Fig. 12. CA curves of (a) 0.1  $\text{CdTe}(50-50)/\text{TiO}_2$  under UV illumination at different potentials, (b) 0.1 %  $\text{CdTe}/\text{TiO}_2$  catalysts under UV illumination at 0.6 V, (c) 0.1 %  $\text{CdTe}(50-50)/\text{TiO}_2$  dark and under UV illumination at 0.6 V, (d) specific activities after 1000 s in 1 M KOH + 0.5 M glucose solution.



**Fig. 13.** Nyquist plots of (a) 0.1 % CdTe(50–50)/TiO<sub>2</sub> under UV illumination in different potentials, (b) 0.1 % CdTe/TiO<sub>2</sub> catalysts under UV illumination at 0.6 V, (c) 0.1 % CdTe(50–50)/TiO<sub>2</sub> catalyst dark and under UV illumination at 0.6 V in 1 M KOH + 0.5 M glucose solution.

[51]. SEM and TEM mapping results showed that Cd and Te metals were homogeneously distributed. In the studies conducted in the literature, they emphasized that the structures were homogeneously distributed when wet impregnation was used as the synthesis method [89–91]. XPS analysis illustrated that the crystal structure and electronic state of the sample have changed. The UV–vis spectrum showed that the bandgap of CdTe/TiO<sub>2</sub> relative to TiO<sub>2</sub> decreased but still remained in the UV region. TPR, TPO, and TPD analyses presented positive or negative shifts in the reduction, oxidation, and adsorption–desorption peaks of TiO<sub>2</sub> when the temperature increased when doped with metal, indicating the presence of metal. The CV, CA, and EIS analyses were performed to the activity, stability, and resistance for photocatalytic glucose electrooxidation measurements of 0.1 % CdTe/TiO<sub>2</sub> catalysts in the dark and UV illumination, respectively. The 0.1 % CdTe(50–50)/TiO<sub>2</sub> catalyst under UV illumination displayed the best photocatalytic activity with a specific activity of 16.88 mA cm<sup>-2</sup> (41798.85 mA mg<sup>-1</sup> Cd) than both the dark (6.22 mA cm<sup>-2</sup>) and other catalysts. It also showed the best stability and resistance for photocatalytic glucose electrooxidation by CA and EIS analyses under UV illumination as in the CV analysis. Although TiO<sub>2</sub> has a wide band gap, it has been observed in literature studies that the photocatalytic activity is increased by decreasing the band gap with CdTe metals. The CdTe–TiO<sub>2</sub> photocatalyst has been used in many areas such as photocatalytic degradation, and they emphasized that the photocatalytic activity increases when CdTe metals are added to the TiO<sub>2</sub> structure [58,92,93]. There are very few studies in the literature for photocatalytic glucose electrooxidation. 0.1 % CdTe(50–50)/TiO<sub>2</sub> catalyst has high catalytic activity in photocatalytic glucose electrooxidation and glucose electrooxidation compared to the literature.

These results are promising as a photoanode catalyst for PFCs with low metal content and high specific and mass photoactivity.

#### CRediT authorship contribution statement

**Aykut Caglar:** Conceptualization, Methodology, Validation, Formal analysis, Investigation, Resources, Data curation, Writing – original draft, Writing – review & editing, Visualization, Supervision, Project administration. **Nahit Aktas:** Methodology, Validation, Formal analysis, Project administration, Funding acquisition. **Hilal Kivrak:** Conceptualization, Methodology, Validation, Formal analysis, Investigation, Resources, Data curation, Writing – original draft, Writing – review & editing, Visualization, Supervision, Project administration, Funding acquisition.

#### Declaration of Competing Interest

The authors declare that they have no known competing financial interests or personal relationships that could have appeared to influence the work reported in this paper.

#### Data availability

The data that has been used is confidential.

#### Acknowledgment

Financial support is gratefully acknowledged from Kyrgyz-Turkish

Manas University with Grant # KTMU-BAP-2019.FBE.05.

## References

- Asongu SA, Agboola MO, Alola AA, Bekun FV. The criticality of growth, urbanization, electricity and fossil fuel consumption to environment sustainability in Africa. *Sci Total Environ* 2020;712:136376.
- Eshghi A, kheirmand M. Graphene/Ni-Fe layered double hydroxide nano composites as advanced electrode materials for glucose electro oxidation. *Int J Hydrogen Energy* 2017;42:15064–72.
- Caglar A, Kivrak H. Highly active carbon nanotube supported PdAu alloy catalysts for ethanol electrooxidation in alkaline environment. *Int J Hydrogen Energy* 2019; 44:11734–43.
- Li X, Wang G, Jing L, Ni W, Yan H, Chen C, et al. A photoelectrochemical methanol fuel cell based on aligned TiO<sub>2</sub> nanorods decorated graphene photoanode. *Chem Commun* 2016;52:2533–6.
- Han L, Guo S, Xu M, Dong S. Photoelectrochemical batteries for efficient energy recovery. *Chem Commun* 2014;50:13331–3.
- Zhao Q, Li Z, Deng Q, Zhu L, Luo S, Li H. Paired photoelectrocatalytic reactions of glucose driven by a photoelectrochemical fuel cell with assistance of methylene blue. *Electrochim Acta* 2016;210:38–44.
- Elouarzaki K, Le Goff A, Holzinger M, Thery J, Cosnier S. Electrocatalytic oxidation of glucose by rhodium porphyrin-functionalized MWCNT electrodes: application to a fully molecular catalyst-based glucose/O<sub>2</sub> fuel cell. *J Am Chem Soc* 2012;134: 14078–85.
- Brouzgou A, Song S, Tsiakaras P. Carbon-supported PdSn and Pd<sub>3</sub>Sn<sub>2</sub> anodes for glucose electrooxidation in alkaline media. *Appl Catal B: Environ* 2014;158–159: 209–16.
- Lu S-J, Ji S-B, Liu J-C, Li H, Li W-S. Photoelectrocatalytic oxidation of glucose at a ruthenium complex modified titanium dioxide electrode promoted by uric acid and ascorbic acid for photoelectrochemical fuel cells. *J Power Sources* 2015;273:142–8.
- Ameta R, Solanki MS, Benjamin S, Ameta SC. Chapter 6 – Photocatalysis. In: Ameta SC, Ameta R, editors. *Advanced Oxidation Processes for Waste Water Treatment*. Academic Press; 2018. p. 135–75.
- Li S, Wang C, Cai M, Yang F, Liu Y, Chen J, et al. Facile fabrication of TaON/Bi<sub>2</sub>MoO<sub>6</sub> core-shell S-scheme heterojunction nanofibers for boosting visible-light catalytic levofloxacin degradation and Cr(VI) reduction. *Chem Eng J* 2022;428: 131158.
- Matsumoto Y. Energy positions of oxide semiconductors and photocatalysis with iron complex oxides. *J Solid State Chem* 1996;126:227–34.
- Liu X, Gu S, Zhao Y, Zhou G, Li W. BiVO<sub>4</sub>, Bi<sub>2</sub>WO<sub>6</sub> and Bi<sub>2</sub>MoO<sub>6</sub> photocatalysis: a brief review. *J Mater Sci Technol* 2020;56:45–68.
- Lu Y, Ou X, Wang W, Fan J, Lv K. Fabrication of TiO<sub>2</sub> nanofiber assembly from nanosheets (TiO<sub>2</sub>-NFs-NSs) by electrospinning-hydrothermal method for improved photoreactivity. *Chin J Catal* 2020;41:209–18.
- Li J, Wu X, Liu S. Fluorinated TiO<sub>2</sub> hollow photocatalysts for photocatalytic applications. *Acta Phys Chim Sin* 2021;37:2009038.
- Li H, Sun B, Gao T, Li H, Ren Y, Zhou G. Ti<sub>3</sub>C<sub>2</sub> MXene co-catalyst assembled with mesoporous TiO<sub>2</sub> for boosting photocatalytic activity of methyl orange degradation and hydrogen production. *Chin J Catal* 2022;43:461–71.
- Liu D, Chen S, Li R, Peng T. Review of Z-scheme heterojunctions for photocatalytic energy conversion. *Acta Phys-Chim Sin* 2021;37:2010017.
- Nishanthi S, Raja DH, Subramanian E, Padiyan DP. Remarkable role of annealing time on anatase phase titania nanotubes and its photoelectrochemical response. *Electrochim Acta* 2013;89:239–45.
- Fujishima A, Honda K. Electrochemical photolysis of water at a semiconductor electrode. *Nature* 1972;238:37–8.
- Chiarello GL, Dozzi MV, Selli E. TiO<sub>2</sub>-based materials for photocatalytic hydrogen production. *J Energy Chem* 2017;26:250–8.
- Zheng L, Teng F, Ye X, Zheng H, Fang X. Photo/electrochemical applications of metal sulfide/TiO<sub>2</sub> heterostructures. *Adv Energy Mater* 2020;10:1902355.
- Pan B, Qin J, Wang C. 6 – Photoreduction of CO<sub>2</sub> on non-TiO<sub>2</sub>-based metal oxides. In: Wang X, Anpo M, Fu X, editors. *Current Developments in Photocatalysis and Photocatalytic Materials*. Elsevier; 2020. p. 77–87.
- Kuvarega AT, Mamba BB. TiO<sub>2</sub>-based photocatalysis: toward visible light-responsive photocatalysts through doping and fabrication of carbon-based nanocomposites. *Crit Rev Solid State Mater Sci* 2017;42:295–346.
- Hu C, Kelm D, Schreiner M, Wollborn T, Mädler L, Teoh WY. Designing photoelectrodes for photocatalytic fuel cells and elucidating the effects of organic substrates. *ChemSusChem* 2015;8:4005–15.
- Chu D, Li XH, Feng DX, Gu JS, Shen G. Electrocatalytic oxidation of glucose on carbon nanotube/nanocrystalline TiO<sub>2</sub> film loaded Pt complex electrode. *Acta Chim Sinica* 2004;62:2403–6.
- Gu Y, Yang H, Li B, Mao J, An Y. A ternary nanooxide NiO-TiO<sub>2</sub>-ZrO<sub>2</sub>/SO<sub>4</sub><sup>2-</sup> as efficient solid superacid catalysts for electro-oxidation of glucose. *Electrochim Acta* 2016;194:367–76.
- Long M, Tan L, Tang AD. The effects of electroplating conditions on the morphology and glucose oxidation performance of Cu<sub>2</sub>O/TiO<sub>2</sub>. *Adv Mater Res* 2014;937:3–8.
- Gu Y, Liu Y, Yang H, Li B, An Y. Electrocatalytic glucose oxidation via hybrid nanomaterial catalyst of multi-wall TiO<sub>2</sub> nanotubes supported Ni(OH)<sub>2</sub> nanoparticles: Optimization of the loading level. *Electrochim Acta* 2015;160: 263–70.
- Caglar A, Ulas B, Sahin O, Demir Kivrak H. Few-layer graphene coated on indium tin oxide electrodes prepared by chemical vapor deposition and their enhanced glucose electrooxidation activity. *Energy Storage* 2019;1:e73.
- Caglar A, Ulas B, Sahin O, Kivrak H. Synthesis of in situ N-, S-, and B-doped few-layer graphene by chemical vapor deposition technique and their superior glucose electrooxidation activity. *Int J Energy Res* 2019;43:8204–16.
- Caglar A, Düzenli D, Onal I, Tezsevin I, Sahin O, Kivrak H. A comparative experimental and density functional study of glucose adsorption and electrooxidation on the Au-graphene and Pt-graphene electrodes. *Int J Hydrogen Energy* 2020;45:490–500.
- Caglar A, Kivrak H, Aktas N, Solak AO. Fabrication of carbon-doped titanium dioxide nanotubes as anode materials for photocatalytic glucose fuel cells. *J Electron Mater* 2021:1–12.
- Caglar A, Aktas N, Kivrak H. Tailoring cadmium composition on titanium dioxide to achieve enhanced photocatalytic glucose fuel cell anode performance. *ACS Appl Energy Mater* 2021;4:12298–309.
- Galińska A, Walendziewski J. Photocatalytic water splitting over Pt–TiO<sub>2</sub> in the presence of sacrificial reagents. *Energy Fuels* 2005;19:1143–7.
- Hamad AR, Calis H, Caglar A, Kivrak H, Kivrak A. Indole-based novel organic anode catalyst for glucose electrooxidation. *Int J Energy Res* 2022;46:1659–71.
- Ma Z, Liu J, Zhu Y, Zhao Y, Lin H, Zhang Y, et al. Crystal-facet-dependent catalysis of anatase TiO<sub>2</sub> on hydrogen storage of MgH<sub>2</sub>. *J Alloy Compd* 2020;822:153553.
- Akdemir M, Avci Hansu T, Caglar A, Kaya M, Demir Kivrak H. Ruthenium modified defatted spent coffee catalysts for supercapacitor and methanolysis application. *Energy Storage* 2021;3:e243.
- Reeves P, Ohlhausen R, Sloan D, Pamplin K, Scoggins T, Clark C, et al. Photocatalytic destruction of organic dyes in aqueous TiO<sub>2</sub> suspensions using concentrated simulated and natural solar energy. *Sol Energy* 1992;48:413–20.
- Pinilla S, Machín A, Park S-H, Arango JC, Nicolosi V, Márquez-Linares F, Morant C. TiO<sub>2</sub>-based nanomaterials for the production of hydrogen and the development of lithium-ion batteries. *J Phys Chem B* 2018;122:972–83.
- Trang TNQ, Nam ND, Ngoc Tu LT, Quoc HP, Van Man T, Ho VTT, et al. In situ spatial charge separation of an Ir@TiO<sub>2</sub> multiphase photosystem toward highly efficient photocatalytic performance of hydrogen production. *J Phys Chem C* 2020; 124:16961–74.
- Xiong Z, Lei Z, Li Y, Dong L, Zhao Y, Zhang J. A review on modification of facet-engineered TiO<sub>2</sub> for photocatalytic CO<sub>2</sub> reduction. *J Photochem Photobiol, C* 2018;36:24–47.
- Yoong LS, Chong FK, Dutta BK. Development of copper-doped TiO<sub>2</sub> photocatalyst for hydrogen production under visible light. *Energy* 2009;34:1652–61.
- Abdel-Baset T, Bashal AH. Structure and AC conductivity of zinc and nickel-doped TiO<sub>2</sub> nanocomposite synthesized by simple incipient wet impregnation method. *J Mater Sci: Mater Electron* 2020;31:18533–40.
- Li W, Zhang M, Du Z, Ma Q, Jameel H, Chang H-M. Photocatalytic degradation of lignin model compounds and kraft pine lignin by CdS/TiO<sub>2</sub> under visible light irradiation. *BioResources* 2015;10:1245–59.
- Qu X, Liu M, Li L, Wang R, Sun H, Shi L, et al. BiOBr flakes decoration and structural modification for CdTe/TiO<sub>2</sub> spheres: Towards water decontamination under simulated light irradiation. *Mater Sci Semicond Process* 2019;93:331–8.
- Huang K, Chen L, Deng J, Xiong J. Enhanced visible-light photocatalytic performance of nanosized anatase TiO<sub>2</sub> doped with CdS quantum dots for cancer-cell treatment. *J Nanomater* 2012;2012:720491.
- Chu S, Zhou W, Zhang C, Zheng Y, Liu Y, Liu Y. Relationship between the structure and catalytic performance of MoS<sub>2</sub> with different surfactant-assisted syntheses in the hydrodesulfurization reaction of 4, 6-DMDBT. *RSC Adv* 2020;10:7600–8.
- Sun S, Li H, Xu ZJ. Impact of surface area in evaluation of catalyst activity. *Joule* 2018;2:1024–7.
- Wang J, Wang G, Cheng B, Yu J, Fan J. Sulfur-doped g-C<sub>3</sub>N<sub>4</sub>/TiO<sub>2</sub> S-scheme heterojunction photocatalyst for Congo Red photodegradation. *Chin J Catal* 2021; 42:56–68.
- Gholap H, Patil R, Yadav P, Banpurkar A, Ogale S, Gade W. CdTe-TiO<sub>2</sub> nanocomposite: an impedor of bacterial growth and biofilm. *Nanotechnology* 2013;24:195101.
- Kim DS, Han SJ, Kwak S-Y. Synthesis and photocatalytic activity of mesoporous TiO<sub>2</sub> with the surface area, crystallite size, and pore size. *J Colloid Interface Sci* 2007;316:85–91.
- Jiang C, Wei M, Qi Z, Kudo T, Honma I, Zhou H. Particle size dependence of the lithium storage capability and high rate performance of nanocrystalline anatase TiO<sub>2</sub> electrode. *J Power Sources* 2007;166:239–43.
- Li Y-S, Jiang F-L, Xiao Q, Li R, Li K, Zhang M-F, et al. Enhanced photocatalytic activities of TiO<sub>2</sub> nanocomposites doped with water-soluble mercapto-capped CdTe quantum dots. *Appl Catal B* 2010;101:118–29.
- Lin X, Xing J, Wang W, Shan Z, Xu F, Huang F. Photocatalytic activities of heterojunction semiconductors Bi<sub>2</sub>O<sub>3</sub>/BaTiO<sub>3</sub>: a strategy for the design of efficient combined photocatalysts. *J Phys Chem C* 2007;111:18288–93.
- San Martín S, Rivero MJ, Ortiz I. Unravelling the mechanisms that drive the performance of photocatalytic hydrogen production. *Catalysts* 2020;10:901.
- Jian L, Jiménez-Calvo P, Paineau E, Ghazzal M. Metal chalcogenides based heterojunctions and novel nanostructures for photocatalytic hydrogen evolution. *Catalysts* 2020;10:89.
- Wang Y, Shi H, Cui K, Yu J. Engineering organic/inorganic hierarchical photocathode for efficient and stable quasi-solid-state photoelectrochemical fuel cells. *Appl Catal B* 2019;250:171–80.
- Li D, Wang S, Wang J, Zhang X, Liu S. Synthesis of CdTe/TiO<sub>2</sub> nanoparticles and their photocatalytic activity. *Mater Res Bull* 2013;48:4283–6.

- [59] Wang X-T, Wei Q-Y, Zhang L, Sun H-F, Li H, Zhang Q-X. CdTe/TiO<sub>2</sub> nanocomposite material for photogenerated cathodic protection of 304 stainless steel. *Mater Sci Eng, B* 2016;208:22–8.
- [60] Luo B, Deng Y, Wang Y, Zhang Z, Tan M. Heterogeneous flammulina velutipes-like CdTe/TiO<sub>2</sub> nanorod array: a promising composite nanostructure for solar cell application. *J Alloy Compd* 2012;517:192–7.
- [61] Deshmane VG, Owen SL, Abrokwah RY, Kuila D. Mesoporous nanocrystalline TiO<sub>2</sub> supported metal (Cu, Co, Ni, Pd, Zn, and Sn) catalysts: Effect of metal-support interactions on steam reforming of methanol. *J Mol Catal A: Chem* 2015;408:202–13.
- [62] Zhang N, Yang Z, Chen Z, Yunxiang L, Liao Y, Li Y, et al. Synthesis of sulfur-resistant TiO<sub>2</sub>-CeO<sub>2</sub> composite and its catalytic performance in the oxidation of a soluble organic fraction from diesel exhaust. *Catalysts* 2018;8.
- [63] Van Doorn J, Vuurman MA, Tromp P, Stufkens D, Moulijn J. Correlation between Raman spectroscopic data and the temperature-programmed oxidation reactivity of coals and carbons. *Fuel Process Technol* 1990;24:407–13.
- [64] Barrie PJ. Analysis of temperature programmed desorption (TPD) data for the characterisation of catalysts containing a distribution of adsorption sites. *Phys Chem Chem Phys* 2008;10:1688–96.
- [65] Zhou M, Liu P, Wang K, Xu J, Jiang J. Catalytic hydrogenation and one step hydrogenation-esterification to remove acetic acid for bio-oil upgrading: model reaction study. *Catal Sci Technol* 2016;6:7783–92.
- [66] Choi H-J, Kim J-S, Kang M. Photodecomposition of concentrated ammonia over nanometer-sized TiO<sub>2</sub>, V-TiO<sub>2</sub>, and Pt/V-TiO<sub>2</sub> photocatalysts. *Korean Chem Soc* 2007;28.
- [67] Chen L, Xu Z, Li J, Zhou B, Shan M, Li Y, et al. Modifying graphite oxide nanostructures in various media by high-energy irradiation. *RSC Adv* 2014;4:1025–31.
- [68] Ivan R, Popescu C, del Pino AP, Yousef I, Logofatu C, György E. Laser-induced synthesis and photocatalytic properties of hybrid organic-inorganic composite layers. *J Mater Sci* 2019;54:3927–41.
- [69] Yan B, Zhou J, Liang X, Song K, Su X. Facile synthesis of flake-like TiO<sub>2</sub>/C nanocomposites for photocatalytic H<sub>2</sub> evolution under visible-light irradiation. *Appl Surf Sci* 2017;392:889–96.
- [70] Li W, Li M, Xie S, Zhai T, Yu M, Liang C, et al. Improving the photoelectrochemical and photocatalytic performance of CdO nanorods with CdS decoration. *CrystEngComm* 2013;15:4212–6.
- [71] Sharma S, Shivaprasad S, Kohli S, Rastogi A. Substrate temperature dependence of electrical conduction in nanocrystalline CdTe: TiO<sub>2</sub> sputtered films. *Pure Appl Chem* 2002;74:1739–49.
- [72] Cao S, Liu T, Tsang Y, Chen C. Role of hydroxylation modification on the structure and property of reduced graphene oxide/TiO<sub>2</sub> hybrids. *Appl Surf Sci* 2016;382:225–38.
- [73] Dolgov A, Lopaev D, Lee C, Zoethout E, Medvedev V, Yakushev O, et al. Characterization of carbon contamination under ion and hot atom bombardment in a tin-plasma extreme ultraviolet light source. *Appl Surf Sci* 2015;353:708–13.
- [74] Xie W, Li R, Xu Q. Enhanced photocatalytic activity of Se-doped TiO<sub>2</sub> under visible light irradiation. *Sci Rep* 2018;8:1–10.
- [75] Zhang Q, Bao N, Wang X, Hu X, Miao X, Chaker M, et al. Advanced fabrication of chemically bonded graphene/TiO<sub>2</sub> continuous fibers with enhanced broadband photocatalytic properties and involved mechanisms exploration. *Sci Rep* 2016;6:1–15.
- [76] Bharti B, Kumar S, Lee H-N, Kumar R. Formation of oxygen vacancies and Ti<sup>3+</sup> state in TiO<sub>2</sub> thin film and enhanced optical properties by air plasma treatment. *Sci Rep* 2016;6:32355.
- [77] Yu J, Gong C, Wu Z, Wu Y, Xiao W, Su Y, et al. Efficient visible light-induced photoelectrocatalytic hydrogen production using CdS sensitized TiO<sub>2</sub> nanorods on TiO<sub>2</sub> nanotube arrays. *J Mater Chem A* 2015;3:22218–26.
- [78] Li W, Li M, Xie S, Zhai T, Yu M, Liang C, Ouyang X, Lu X, Li H, Tong Y. Improving the photoelectrochemical and photocatalytic performance of CdO nanorods with CdS decoration. *CrystEngComm* 2013;15:4212–6.
- [79] Yu X-Y, Lei B-X, Kuang D-B, Su C-Y. Highly efficient CdTe/CdS quantum dot sensitized solar cells fabricated by a one-step linker assisted chemical bath deposition. *Chem Sci* 2011;2:1396–400.
- [80] Sharma S, Shivaprasad S, Kohli S, Rastogi A. Substrate temperature dependence of electrical conduction in nanocrystalline CdTe:TiO<sub>2</sub> sputtered films. *Pure Appl Chem* 2002;74:1739–49.
- [81] Masood HT, Muhammad Z, Habib M, Wang D-M, Wang D-L. Low temperature ferromagnetic properties of CdS and CdTe thin films. *Chin Phys B* 2017;26:067503.
- [82] Manikandan M, Revathi C, Senthilkumar P, Amreetha S, Dhanuskodi S, Kumar RR. CdTe nanorods for nonenzymatic hydrogen peroxide biosensor and optical limiting applications. *Ionics* 2020;26:2003–10.
- [83] Huang K, Chen L, Deng J, Xiong J. Enhanced visible-light photocatalytic performance of nanosized anatase TiO<sub>2</sub> doped with CdS quantum dots for cancer-cell treatment. *J Nanomater* 2012;2012.
- [84] Liqiang J, Yichun Q, Baiqi W, Shudan L, Baojiang J, Libin Y, et al. Review of photoluminescence performance of nano-sized semiconductor materials and its relationships with photocatalytic activity. *Sol Energy Mater Sol Cells* 2006;90:1773–87.
- [85] Hansu TA, Caglar A, Sahin O, Kivrak H. Hydrolysis and electrooxidation of sodium borohydride on novel CNT supported CoBi fuel cell catalyst. *Mater Chem Phys* 2020;239:122031.
- [86] Caglar A, Cogenli MS, Yurtcan AB, Kivrak H. Effective carbon nanotube supported metal (M=Au, Ag, Co, Mn, Ni, V, Zn) core Pd shell bimetallic anode catalysts for formic acid fuel cells. *Renewable Energy* 2020;150:78–90.
- [87] Ulas B, Caglar A, Sahin O, Kivrak H. Composition dependent activity of PdAgNi alloy catalysts for formic acid electrooxidation. *J Colloid Interface Sci* 2018;532:47–57.
- [88] Caglar A, Aktas N, Kivrak H. Tailoring cadmium composition on titanium dioxide to achieve enhanced photocatalytic glucose fuel cell anode performance. *ACS Appl Energy Mater* 2021.
- [89] Alcalá MD, Real C. Synthesis based on the wet impregnation method and characterization of iron and iron oxide-silica nanocomposites. *Solid State Ionics* 2006;177:955–60.
- [90] Zhang C, Oliaee SN, Hwang SY, Kong X, Peng Z. A generic wet impregnation method for preparing substrate-supported platinum group metal and alloy nanoparticles with controlled particle morphology. *Nano Lett* 2016;16:164–9.
- [91] Jiang SP. A review of wet impregnation—an alternative method for the fabrication of high performance and nano-structured electrodes of solid oxide fuel cells. *Mater Sci Eng, A* 2006;418:199–210.
- [92] Feng H, Tran T, Chen TL, Yuan L, Cai Q. Visible light-induced efficiently oxidative decomposition of p-Nitrophenol by CdTe/TiO<sub>2</sub> nanotube arrays. *Chem Eng J* 2013;215–216:591–9.
- [93] Gong Y, Wu Y, Xu Y, Li L, Li C, Liu X, et al. All-solid-state Z-scheme CdTe/TiO<sub>2</sub> heterostructure photocatalysts with enhanced visible-light photocatalytic degradation of antibiotic waste water. *Chem Eng J* 2018;350:257–67.